Control of Peptide Amphiphile Supramolecular Nanostructures by Isosteric Replacements

*Huihua Xing,[a] Stacey M. Chin,[b] Venkata Reddy Udumula,[a] Krishnaiah Maddeboina,[a] Nathalia Rodrigues de Almeida,[a]† Cristián Huck-Iriart,[c] Agustín S. Picco,[d] Sieun Ruth Lee,[b] Gervasio Zaldivar,[e] Kelsey A. Jackson,[f] Mario Tagliazucchi,[e] Samuel I. Stupp,[g] and Martin Conda-Sheridan[a]**

[a] College of Pharmacy, University of Nebraska Medical Center, Omaha, NE 68105, USA
[b] Department of Chemistry, Northwestern University, Evanston, IL 60208, USA
[c] Laboratorio de Cristalografía Aplicada, Escuela de Ciencia y Tecnología, Universidad Nacional de General San Martín, Buenos Aires, Argentina
[d] Instituto de Investigaciones Fisicoquímicas Teóricas y Aplicadas, INIFTA-CONICET-UNLP, La Plata, Argentina
[e] INQUIMAE-CONICET and DQIAQF, Universidad de Buenos Aires, Facultad de Ciencias, Ciudad Universitaria, Ciudad de Buenos Aires, Argentina
[f] College of Arts and Sciences, Creighton University, Omaha, NE 68178, USA
[g] Department of Materials Science & Engineering, Chemistry, Biomedical Engineering, Medicine, and Simpson Querrey Institute, Northwestern University, Evanston, IL 60208, USA

Email: martin.condasheridan@unmc.edu
Phone: +1 402-559-9361

KEYWORDS: self-assembly, peptide amphiphile, nanostructures, isotere

ABSTRACT: Supramolecular nanostructures with tunable properties can have applications in medicine, pharmacy, and biotechnology. On this work, we show that the self-assembly behavior of peptide amphiphiles (PA) can be effectively tuned by replacing the carboxylic acids exposed to the aqueous media with isosteres, functionalities that share key physical or chemical properties with another chemical group. Transmission electron microscopy, atomic force microscopy, and small-angle X-ray scattering studies indicated that the nanostructure's morphologies are responsive to the ionization states of the side chains, which are related to their pK_a values. Circular dichroism studies revealed the effect of the isosteres on the internal arrangement of the nanostructures. The interactions between diverse surfaces and the nanostructures and the effect of salt concentration and temperature were assessed to further understand the properties of these self-assembled systems. These results indicate that isosteric replacements allow the pH control of supramolecular morphology by manipulating the pKa of the charged groups located on the nanostructure's surface. Theoretical studies were performed to understand the morphological transitions the nanostructures underwent in response to pH changes, suggesting the transitions result from alterations in the Coulomb forces between PA molecules. This work provides a strategy for designing biomaterials that can maintain or change behaviors based on the pH differences found within cells and tissues.

1. Introduction

The self-assembly process consists on the spontaneous organization of small building blocks into highly-ordered supramolecular structures.[1-3] Among the reported self-assembling molecules, peptide amphiphiles (PAs) have become particularly attractive due to their potential therapeutic applications, including drug and protein delivery,[4-6] regenerative medicine,[1, 7-9] and as nanodrugs to treat cancer and bacterial infections.[10-12] Two decades ago, Samuel Stupp and his group developed a class of PAs that assemble into high-aspect-ratio nanofilaments.[13] These PA molecules are composed of a hydrophobic alkyl tail connected to a peptide sequence that can form β-sheet interactions and a charged portion to enhance water solubility. The more complex PA nanostructures contain a bioactive epitope for targeting or cell signaling.[13-15]

To control these supramolecular assemblies, it is necessary to understand how the PAs respond to pH, salt concentration, solvent, or heat changes. Seminal works from the groups of Stupp,[16, 17] Meijer,[18] Goldberger,[19, 20] and Guler[21, 22] have highlighted the effect of pH, media, and processing on supramolecular architecture. Meanwhile, the group of Shen[23] has shown that a decrease in electrostatic repulsions shifts the morphology from micelles to fibers. Further, Zaldivar et al. [24] combined experiments with a Molecular Theory (MOLT) to demonstrate that controlling the pH of the solution triggers a micelle-fiber-lamella transition.

Thus, to enhance function *in operando*, it is necessary to understand the effect of external conditions on the characteristics of a supramolecular system. This information can then be used to enhance the stability of the nanostructure against an external stimulus (pH, temperature, ionic strength) or to create nanostructures that respond to environmental cues (i.e. supramolecular transition at a desired location).[25-27] An unexplored strategy to achieve such control is the use of isosteric replacements. Isosteres are used in medicinal chemistry to modulate physicochemical

characteristics such as size, electronegativity, topology,[28] as well as solubility and metabolism.[29] In this work, we have merged medicinal chemistry with materials science to develop novel self-assembling materials. We hypothesized the pK_a values of solvent-exposed charged groups should influence the supramolecular morphology and stability in response to pH. We synthesized six PA molecules with anionic headgroups of various pK_a values to assess their self-assembly properties under diverse conditions. All PA molecules had the same hydrophobic segment (C_{16}) covalently conjugated to an amino acid sequence (V_2A_2), which has been previously shown to promote the formation of elongated nanostructures at physiological pH.[23] Through detailed experimental characterization and theoretical modeling of these six anionic PAs, we systematically investigated how groups with different pK_a values respond to the environment (i.e. pH, salt concentration, surface charge) and the effect they exert on the supramolecular behavior.

2. Experimental Section

Materials: Solvents and coupling agents were purchased from Fisher Chemical. Fmoc-amino acids and coupling reagents were obtained from P3Bio (Louisville, KY). Fmoc-Rink Amide AM resin (0.61mmol/g) was purchased from CreoSaulus (Louisville, KY). Fmoc-*L*-Cysteic acid, and Fmoc-Ser(PO_3BzlH)-OH were purchased from Combi-Blocks. The different buffers were prepared as shown in **Table S1**.

Synthesis and characterization of PAs: Isosteric amino acids were synthesized and characterized as described in the **SI** (experimental procedures section). The PAs were prepared using standard Fmoc solid-phase peptide synthesis (SPPS) on a 0.3 mmol scale on Fmoc-Rink Amide AM resin and using HBTU/DIPEA (or DIC/DIPEA) as coupling reagents as published or as indicated in the **SI**.[12] The PAs were purified and characterized as reported.[12, 24] The purities of

the fractions containing the desired PAs were confirmed by analytical HPLC (Agilent) using a C_{18} Kinetex column [5μm XB-C18 100 Å, 250 × 4.6 mm] (Phenomenex). The UV detector was set at 220 nm wavelength and elution was achieved with a linear gradient of ACN/H_2O (both containing 0.1% ammonium hydroxide) from 5 to 95% for 25 min. The fractions with a purity >95% were combined, the organic solvent removed under vacuum, the pH adjusted to 7.0 (0.1 M HCl or NaOH), and the solution lyophilized (FreeZone, Labconco).

Self-assembly: Lyophilized PAs were dissolved in water (2 mg/mL), annealed at 80ºC for 2 h and cooled to room temperature. Samples were diluted with the desired media to achieve a final concentration as 1 mg/mL and aged for 24 h before testing. The final pH was measured using a pH meter. Additions details can be found in **Scheme S1**.

Transmission Electron Microscopy: The PAs in different pH buffers (1 mg/mL) were prepared and aged for 24 h. Approximately, 6 μL of the sample were applied into a copper grid and allowed to absorb for 5 min, covered with a folded piece of filter paper. The excess PA was removed by touching the edge of the grid with a clean piece of the filter paper. Then, 6 μL of the negative stain (NanoVan) was added and the system incubated for 30 sec. The excess stain was blotted off as before, and the sample incubated for 5 min. PAs were visualized with a FEI Tecnai G2 Spirit TEM (120kV). Images were acquired by an AMT digital imaging system.

Cryogenic Transmission Electron Microscopy: 300-mesh copper grids with lacey carbon support (Electron Microscopy Sciences) were glow discharged for 15 s using a PELCO easiGlow Glow Discharge Cleaning System (Ted Pella) and used immediately. The samples were prepared via plunge freezing using a Vitrobot Mark IV (FEI) vitrification robot at room temperature and 90-100% humidity. 7 μL of annealed PA solution (1 mg/mL) was placed on the copper grid, blotted, and plunge frozen into liquid ethane. Samples were transferred immediately into a liquid nitrogen

bath and held until imaging. During imaging, samples were moved into a Gatan 626 cryo-holder through a cryo-transfer stage. The study was performed using a JEOL 1230 TEM working at 100 kV accelerating voltage and the images were obtained with a Gatan 831 CCD camera.

Experimental details for **Small-Angle X-ray scattering (SAXS)**, **Circular Dichroism (CD)**, **Atomic Force Microscopy (AFM)**, and ***In Situ* AFM** can be found on the Supporting Information section.

3. Results and discussion

PA design and characterization

Our objective was to assess the effect of carboxylic acid isosteres in supramolecular self-assembly. We prepared six PAs[12, 30] composed of an alkyl chain (C_{16}), a β-sheet promoting sequence (V_2A_2), and a hydrophilic head (R) (**Figure 1A**). The charged group, R, was either a carboxylic acid (**PA-COOH**, $pK_a \approx 4.8$)[31] or one of its isosteres: sulfonic acid (**PA-SO_3H**, reported pK_a ranges from -1 to -6),[32-34] phosphoric acid (**PA-OPO_3H_2**, $pK_{a1} \approx 2.1$, $pK_{a2} \approx 7.2$-8.5),[28, 35] cyanamide (**PA-CONHCN**, $pK_a = 3.8$),[36] methyl sulfonamide (**PA-$CONHSO_2CH_3$**, $pK_a = 4.94$),[28] or trifluoromethyl sulfonamide (**PA-$CONHSO_2CF_3$**, $pK_a = 3.04$ calculated with MarvinSketch[37]).

The PAs were dissolved in water (pH adjusted to 7.4), and their supramolecular shape studied by cryogenic transmission electron microscopy (cryo-TEM), AFM and small angle X-ray scattering (SAXS). The cryo-TEM shows that **PA-COOH**, **PA-SO_3H**, **PA-OPO_3H_2** and **PA-CONHCN** formed elongated twisted ribbons (**Figure 1B** and **Figure S2**). **PA-COOH** exhibited the widest ribbons (width ~31 nm), while narrower ones were observed for **PA-SO_3H**, **PA-OPO_3H_2** and **PA-CONHCN** (width ~15-17 nm). On the other hand, **PA-$CONHSO_2CH_3$** and **PA-$CONHSO_2CF_3$** assembled into thin ribbons (or nanofibers), with diameters of ~11 nm. The

difference in width seems to be related to the bulkiness of the side chain (except for **PA-SO$_3$H**, **Table S2**). AFM also showed the presence of elongated nanostructures (**Figure S3**).

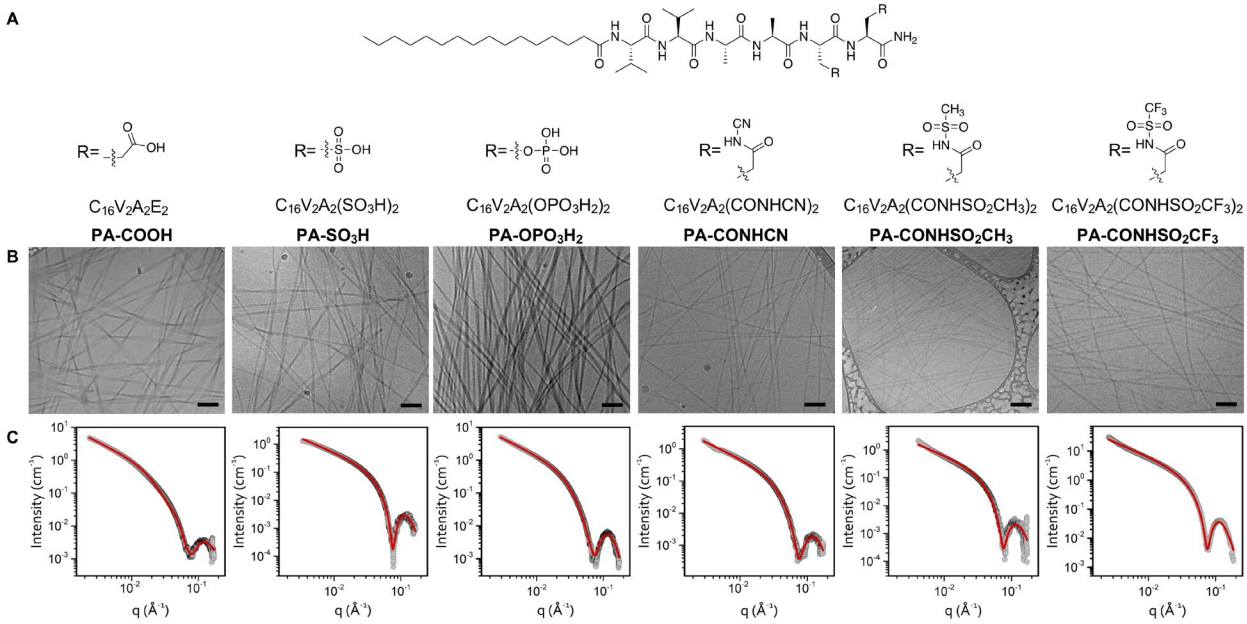


Figure 1. A) Chemical structures of the peptide amphiphiles (PAs) studied in this work. The chemical structure of the 6 different R groups and the nomenclature used for the derived PAs are shown: $C_{16}V_2A_2E_2$ (**PA-COOH**), $C_{16}V_2A_2(SO_3H)_2$ (**PA-SO$_3$H**), $C_{16}V_2A_2(OPO_3H_2)_2$ (**PA-OPO$_3$H$_2$**), $C_{16}V_2A_2(CONHCN)_2$ (**PA-CONHCN)**, $C_{16}V_2A_2(CONHSO_2CH_3)_2$ (**PA-CONHSO$_2$CH$_3$)**, and $C_{16}V_2A_2(CONHSO_2CF_3)_2$ (**PA-CONHSO$_2$CF$_3$)**. B) Cryo-TEM images of PAs. Black lines in the lower right corner of cryo-TEM images represent the scale bars (100 nm). Original figures are shown in **Figure S3**. C) SAXS curves of PAs self-assembled in water. The grey points represent the raw data, and the red curves show the best fit obtained by a model of an infinite ribbon with rectangular core-shell cross section (see text and SI). All samples were prepared in milli-Q water, at 1 mg/mL, and the pH was adjusted to 7.4.

The SAXS curves of all the PAs presented low angle (Guinier) regions with slopes between -1 and -1.5; a key signature of elongated objects.[38, 39] The SAXS data were modeled using a core–shell ribbon model (details can be found in the SI). The analysis indicates that **PA-COOH** forms the widest nanostructures (~26 nm) while the other PAs exhibited lower values: 13-19 nm. Only the width of **PA-SO$_3$H**, measured by SAXS, is smaller than the one measured by microscopy. The results are summarized in **Table 1** and **Tables S2** and **S3**. The height of the nanostructures was similar in SAXS and AFM (ranging from 4.3-7.8 nm) with only **PA-CONHSO$_2$CH$_3$** and **PA-**

$CONHSO_2CF_3$ being shorter by AFM. These two PAs do not present the twisted morphology. Further, their height (~4.7 nm) may suggest the nanofibers have interdigitated alkyl tails.[40]

Table 1. Width of PAs measured by SAXS, AFM and Cryo-TEM

PA	Cryo-TEM (nm)	SAXS (nm)	AFM (nm)	
			Width	Height
PA-COOH	31.4 ± 8.6	25.7 ± 0.4	32.0 ± 4.6	6.8 ± 1.3
PA-SO_3H	15.8 ± 5.4	12.7 ± 0.2	15.5 ± 0.9	6.1 ± 0.6
PA-OPO_3H_2	17.5 ± 4.1	18.6 ± 0.6	24.9 ± 4.1	6.4 ± 0.4
PA-CONHCN	15.3 ± 2.4	15.3 ± 0.1	17.6 ± 0.2	6.2 ± 0.6
PA-$CONHSO_2CH_3$	9.9 ± 1.4	14.6 ± 0.3	13.5 ± 4.0	5.5 ± 0.2
PA-$CONHSO_2CF_3$	11.1 ± 1.6	12.0 ± 1.8	12.8 ± 0.8	4.3 ± 0.5

pH effect on the morphology and secondary structure

Next, we studied the effect of pH (1, 4, 6 and 9) on self-assembly by TEM. At pH = 1, **PA-COOH** formed amorphous aggregates that may be attributed to the carboxylic acid pK_a (~4.8), which makes the PA heads neutral at pH = 1 (pH 1: ~0.016% ionization). The decrease in the electrostatic repulsion between PA molecules leads to the formation of aggregates. At pH = 4 (~15.85% ionization), **PA-COOH** formed a mixture of short ribbons and micelles, while twisted ribbons were seen at pH 6 and 9. **PA-SO_3H** formed elongated nanostructures at all pHs (**Figure 2B**). This can be explained by considering the pK_a of the sulfonate group (< 0), which enables the isostere to be fully deprotonated at all pHs. **PA-OPO_3H_2** also showed short fiber-like structures at pH = 1 but high aspect ratio nanostructures at pH = 4, presumably because the head group is negatively charged at the later pH (pka_1 ~ 2.1). At pH = 6 twisted ribbons are present. Further, we observed that **PA-OPO_3H_2** displayed some shorter ribbons at pH = 9. This may be related to the partial deprotonation of the second hydroxyl group on the phosphoric acid (pK_{a2} ~ 7.2), which could increase Coulomb repulsions that disrupts the ribbons. To confirm this observation, we performed TEM at pH 11 and 12 (**Figure S4**). We observed long and short elongated structures, which further suggest the increased repulsion caused by the second deprotonation prevents the

formation of long ribbons (although we expected to see spheres due to the repulsion). **PA-CONHCN**, **PA-CONHSO$_2$CH$_3$** and **PA-CONHSO$_2$CF$_3$** also show shorter structures at pH = 1. This is more evident in **PA-CONHSO$_2$CH$_3$** which possesses a pK$_a$ of ~ 4.9. At pHs = 4, 6 and 9 these PAs formed twisted ribbons or fibers (in some cases it was difficult to appreciate if twisting was present).

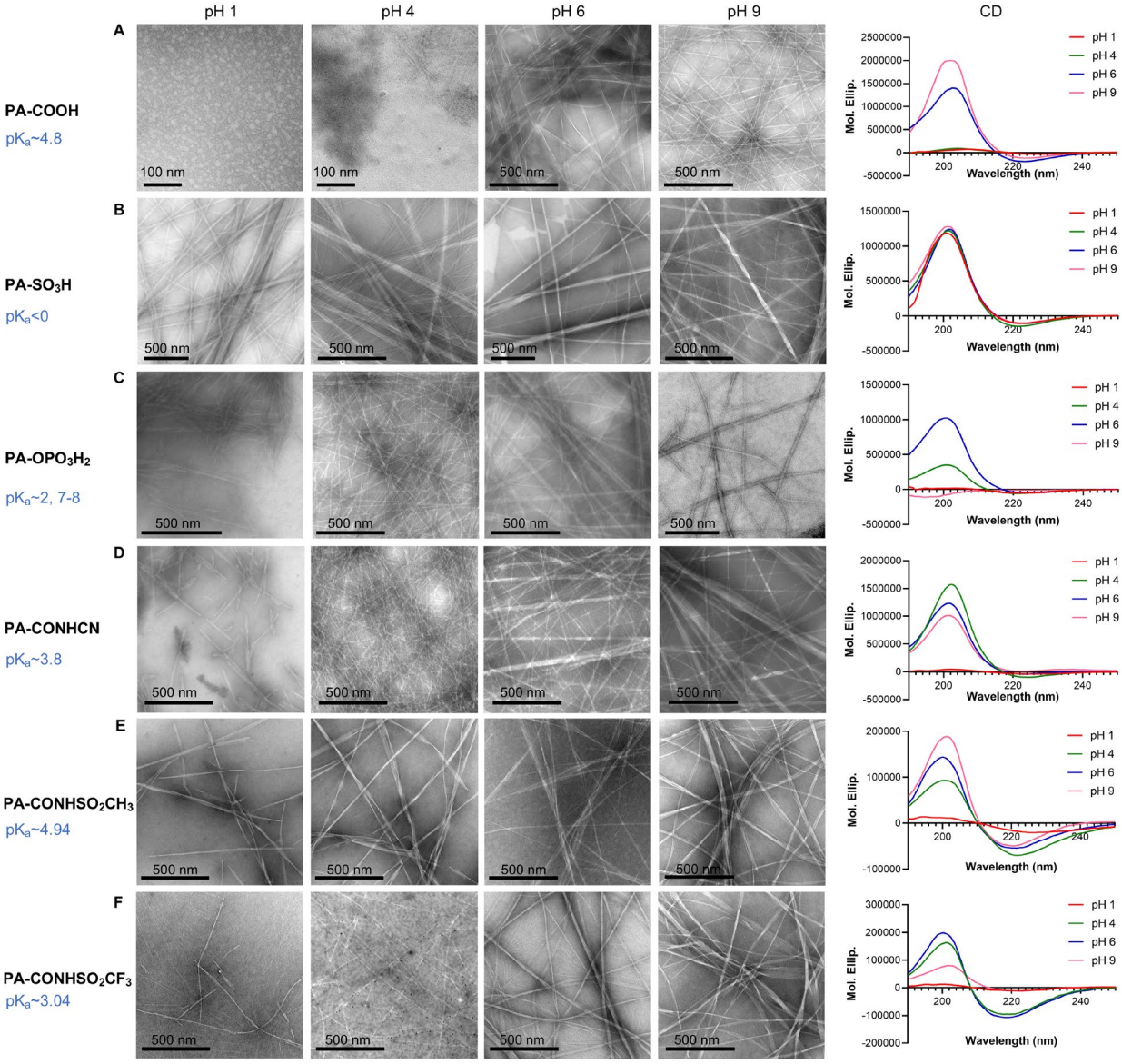


Figure 2. Transmission electron microscopy images (TEM; first four columns from left to right) and circular dichroism spectra (CD; right side column, Molar Ellipticity: deg cm^2 dmol^{-1}) of A) **PA-COOH**, B) **PA-SO$_3$H**, C) **PA-OPO$_3$H$_2$**, D) **PA-CONHSO$_2$CH$_3$**, E) **PA-CONHSO$_2$CF$_3$**, and F) **PA-CONHCN** at pH = 1, 4, 6 and 9. Samples were prepared at 1 mg/mL and aged for 24 h.

Next, we performed *in situ* AFM on 4 of the PAs to understand if a preformed morphology will respond to changes in pH. As can be seen in **Figure S5**, **PA-COOH**, **PA-SO_3H**, and **PA-OPO_3H_2**, and **PA-CONHCN** all formed fibers at pH 6, in agreement with the cryo-TEM data (although some short fibers were also seen in this experiment). When the buffer was replaced (pH lowered to 1) the PAs with pKa< pH changed shape, giving rise to short supramolecular structures. The observed results are consistent with the pH 1 cryo-TEM.

Next, we studied **PA-COOH**, **PA-SO_3H**, and **PA-OPO_3H_2** using SAXS (**Figure S6**; pH = 1, 6, 9). We selected these three PAs because of their pKa differences. At pH = 1, **PA-COOH** and **PA-OPO_3H_2** showed Guinier regions with slopes around -2, a signature of flat assemblies (the cryo TEM shows small structures). At pH 6, the slope of **PA-COOH** is around -2 (but not as pronounced as in the previous case) but for **PA-OPO_3H_2** is closer to -1 than -2. At pH = 9, both **PA-COOH** and **PA-OPO_3H_2** exhibited curves with slopes close to -1 in the low angle region, indicating the formation of high aspect ratio assemblies. On the other hand, **PA-SO_3H** exhibited slopes of -1 at all pHs, which is consistent with the unaltered long ribbon morphology (**Figure 2B**). Thus, the pH studies by TEM and SAXS indicate that the lower the pK_a of the head group, the stronger its ability to prevent supramolecular transitions.

In addition, we studied how pH can alter the secondary structure of the assemblies (**Figure 2**, right side column). The CD spectra of elongated PA nanostructures typically presents β-sheet positive bands at ~ 200 nm and negative ones around 220 nm.[13, 16] The changes on secondary structure could indicate an internal re-arrangement, which can be associated with morphological and/or assembly-disassembly transitions.[18, 41] **PA-COOH** lacked a secondary structure at pHs 1 and 4 but exhibited β-sheets peaks at pHs 6 and 9. This correlates with the TEM and SAXS, where

irregular aggregates are seen at pHs 1 and 4 while twisted ribbons are present at pHs 6 and 9. Supporting what was observed by TEM and SAXS, the CD spectra of **PA-SO_3H** remained almost unaltered at pHs 1 to 9. **PA-OPO_3H_2**, presented β-sheet peaks at pHs 4 and 6 (long ribbons by TEM) and no clear CD features at pH 1. At pH 9, the CD spectra of **PA-OPO_3H_2** was compatible with a random coil (negative peak below 200 nm).[18] As commented, **PA-OPO_3H_2** exhibited shorter ribbons due to the strong intermolecular repulsion at high pH. The remaining PAs: **PA-CONHCN**, **PA-$CONHSO_2CH_3$** and **PA-$CONHSO_2CF_3$** exhibited poorly defined β-sheet peaks at pH = 1 but well-defined peaks at higher pHs (elongated nanostructures by TEM). Notably, these three PAs formed some fiber-like structures at the lowest pHs even in the absence β-sheets. Further, the maxima of the three PAs did not increase with pH indicating that other factors, besides the pKa, play a role on the internal arrangement. We also performed Infrared (IR) studies on the powders and were able to observe peaks that can be ascribed to β-sheet signals, the experiment is detailed in **Figures S7, S8**.

As described, some PAs form aggregates when pKa<pH. This can be caused by (1) the collapse of the nanostructures as they lose colloidal stability at low pH or (2) by the agglomeration of the molecules into disordered aggregates due to reduced water solubility. The first hypothesis is supported by a theoretical model (see below) that predicts that PA nanostructures lose colloidal stability (*i.e.,* aggregation is thermodynamically favored) at pH values similar to those where aggregates are observed in the TEM images (**Figure 2**). This is consistent with the fact that the nanostructures of **PA-COOH** at pH 4 and **PA-OPO_3H_2** at pH 1 seem to be composed of aggregated lamellar objects. Note that it is unlikely that the aggregates observed for **PA-COOH** at pH 1 are the result of a ribbon-to-micelle transition as this transition takes place with increased PA charge (more repulsions).[24, 42] As a general rule, it can be said that when pH > pK_a of head

group, β-sheets features are observed by CD and elongated nanostructures are evidenced by TEM and AFM. Contrarily, when pH < pK_a of head group, there is a lack of secondary structure and aggregates are formed. Please note that other factors, besides the pK_a (i.e., H-bonds provided by the side chains, bulkiness of the side chain, hydrophobicity) may play a key role on the formation and structure of the supramolecular assemblies.

Effect of charge screening

We selected four of the PAs and studied if the ionic strength of the media affects the supramolecular morphology. The addition of NaCl to a pH 7 solution did not affect the shape of the nanostructures formed by **PA-COOH**, **PA-SO_3H** and **PA-CONHCN** (**Figure S9**). However, **PA-OPO_3H_2** showed needle-like structures, slightly shorter than what was observed before (**Figure S10**). Next, we performed cryo-TEM and AFM at pH 10 without and with the addition of NaCl. As can be seen in **Figure 3** and **Figure S11**, the PAs maintained their elongated morphology. **PA-OPO_3H_2** still showed the presence of some shorter fibers, presumably due to repulsions due to deprotonation but the addition of NaCl seemed to increase the length of the fibers. This can be rationalized by the fact the negative charges may be more sensitive to the higher ionic content in the solution. A difference was observed on the cryo-TEM image of **PA-CONHCN**, which showed an increase in width when salt is added. The results described herein indicated that (overall) salt concentration does not have a significant effect of the morphology of the nanostructures formed by the PA-isosteres under the tested conditions.[24]

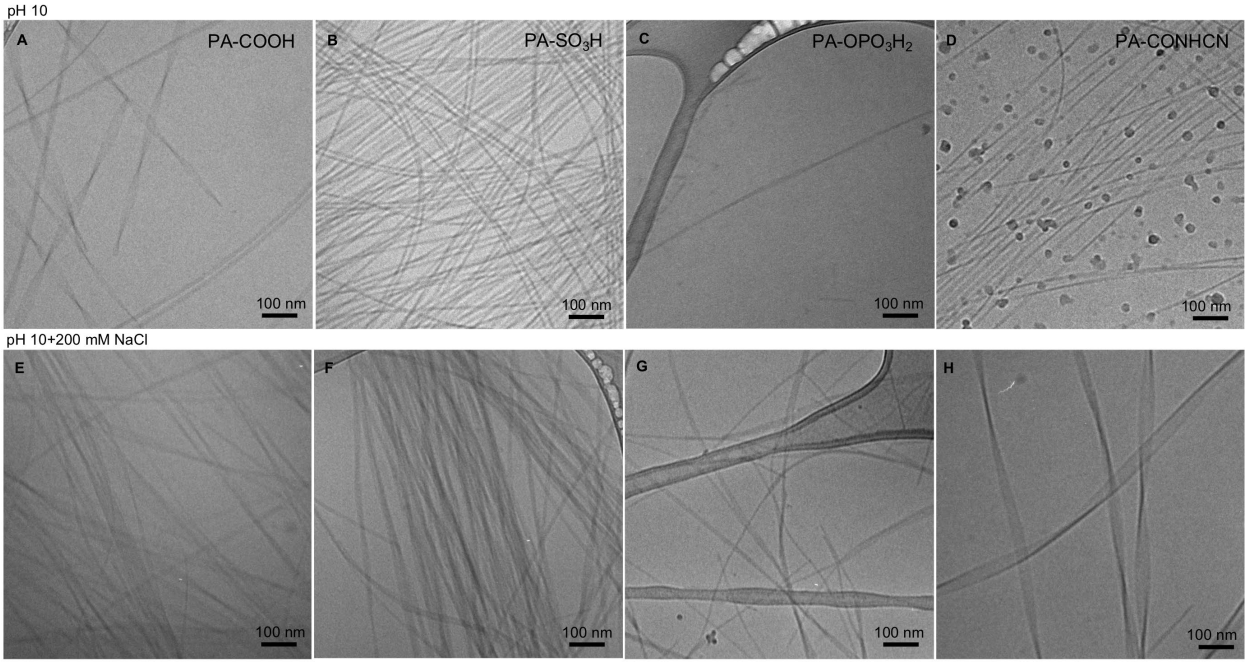


Figure 3. Cryo-TEM images of A, E) **PA-COOH;** B, F) **PA-SO_3H**; C, G) **PA-OPO_3H_2**; D, H) **PA-CONHCN** at pH 10 (50 mM glycine- 32 mM NaOH buffer; 1 mg/mL concentration) without and with NaCl (200 mM), respectively. Scare bar 100 nm.

Structural studies in charged surfaces

Next, we decided to assess how a positively charged surface affects supramolecular morphology by altering the mica (used in AFM) and the grid (TEM). We studied **PA-COOH**, **PA-SO_3H** and **PA-OPO_3H_2** due to their diverse pKas. We found that at pH 1, **PA-COOH** assembles into short ribbons (**Figure S12)** instead of aggregates (**Figure 2A**). This is possibly due to the electrostatic interactions with the cationic surfaces, which were not present before functionalization. At pHs 6 and 9, we saw elongated nanostructures. **PA-SO_3H** provided elongated structures at all the pHs (**Figure S13**) also consistent with the earlier TEM study (**Figure 2B**). Although, at pH 9 we still observed some short, entangled ribbons by AFM. **PA-OPO_3H_2** presented shorter fibers (and perhaps some aggregates) at pHs 1 and 9 (compare **Figures 2C** and **4**) but elongated objects at pH 6. Altogether, the results of the study show that surface charge has a minimal effect on the supramolecular shape of the PAs.

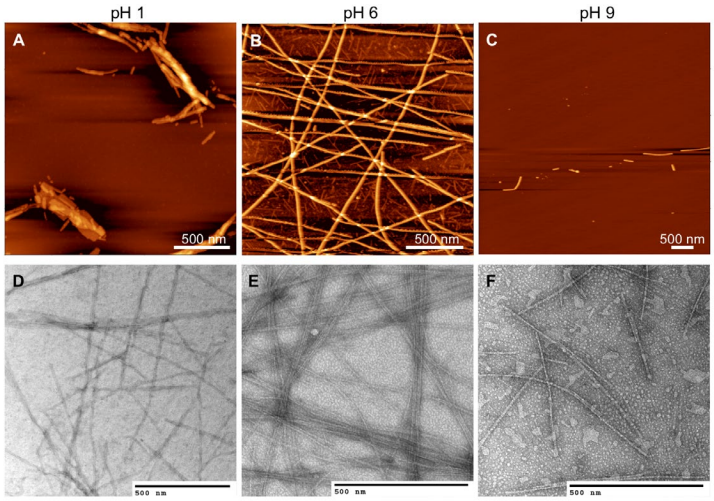


Figure 4. A-C) AFM images and D-F) TEM images (scale bar 500 nm) of **PA-OPO$_3$H$_2$** on positively charged surface at pH 1, 6, and 9, respectively.

Effect of temperature

Then, we performed variable temperature SAXS (25- 90°C, pH = 7.4) to evaluate the thermal stability of selected the nanostructures (**Figure S14**). The stability rank was **PA-SO$_3$H** ~ **PA-OPO$_3$H$_2$** < **PA-CONHCN** < **PA-COOH** (see SI for details). Based on the results, we hypothesize the stability is related to the width of the self-assembled structures (**PA-COOH** is the widest). A potential explanation is that thinner ribbons possess less molecules within its cross section, which translates to less interactions (fewer H-bonds) leading to a decrease in stability. An alternative explanation is related to the increased motion of water at higher temperatures. The temperature weakens H-bonding between the PAs and the water molecules leading to a decrease in charge screening. This increases the charge repulsion causing a morphological transition. Since **PA-COOH** is the molecule with less potential H-bonds on the head group — among the studied PAs— it may have less associated water molecules. This results into less charge screening and a less noticeable temperature-induced change. **PA-SO$_3$H** and **PA-OPO$_3$H$_2$** have a higher number of

oxygens, and the resulting associated waters. The reduced charge screening, due to water movement, will increase the repulsive forces promoting a morphological transition. Based on the NaCl experiments that showed the limited effect that salt has on the morphology, we theorize the first hypothesis, stability is related to the cross section of the PAs, is the most likely explanation.

Theoretical calculations of the PA aggregation

We used a MOLT approach to explain if the observed morphologies are the result of the competition between hydrophobic attractive interactions and a decrease in Coulomb repulsions (See **Figure S15** and associated text for details). We hypothesized that at low pH the ribbons "stick together" because the acidic groups of the PAs are protonated, making the Coulomb repulsions negligible. To test the hypothesis, we calculated the free energy of two approaching ribbons as a function of pH. The free-energy estimation was done using our previously reported model,[24] which explicitly incorporates the molecular details of the PAs (molecular structure, conformations, volume and charge distribution, inter and intramolecular interactions) and the properties of the solution (pH, ionic strength). **Figure 5A** shows the free energy per unit area of two lamellar ribbons formed by **PA-COOH**, $\Delta\Omega^*$, as a function of the distance between them, d. The free energy is defined with respect to that of two lamellas infinitely separated, $\Delta\Omega^* = \Omega^*(d) - \Omega^*(d\rightarrow\infty)$. For pH $\geq$ 6, the free energy increases as the ribbons approach, indicating that the formation of a super-aggregate of ribbons is unstable. For pH $\leq$ 5, the free energy reaches a global minimum at $d \sim 5.5$ nm, which indicates that the aggregated state is stable.

The model predicts a transition from isolated ribbons to ribbon aggregates at pH ~ 5. We speculate that ribbon aggregation can lead to amorphous aggregates or precipitation. To support this interpretation, we show in the inset of **Figure 5A** our prediction for the fraction of charged carboxylate groups, a = [PACOO-]/([PACOOH] + [PACOO-]), as a function of the pH. The fraction was using the approach reported in our previous work.[24] At low pH, all carboxylate groups are uncharged (α ~ 0, inset of **Figure 5A**) and the ribbons stick together due to hydrophobic attractions. An increase in pH increases the fraction of charged carboxylates (see α on insert) and, consequently, the Coulomb repulsions disfavoring the PA-nanostructures approaching each other. At pH ~ 6 (α ~ 0.5), the repulsions are high enough to balance the hydrophobic attractions, and the aggregate becomes "unstable". Note that the pK_a is higher within the individual elongated ribbon (apparent pK_a ~ 6, see inset of **Figure 5A**) than in bulk solution (pK_a ~ 4.8). This pK_a shift is due to a charge regulation effect that has been reported in the literature.[24]

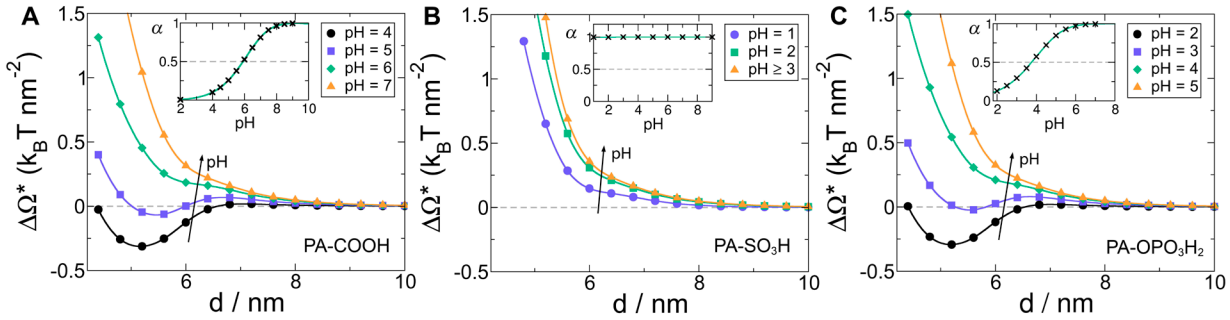


Figure 5. Free energy per unit of area, ΔΩ*, of two ribbons of A) **PA-COOH**, B) **PA-SO₃H** and C) **PA-OPO₃H₂** as a function of the distance between them, *d*, at different pH values. ΔΩ* is defined with respect to the free energy of two infinitely separated ribbons. The insets show the fraction of carboxylate groups, sulfonate groups and phosphonate groups that are deprotonated, α, as a function of pH. The salt concentration was set to 0.1 M in all calculations.

All PAs showed the same behavior than **PA-COOH** except for **PA-SO₃H**, which possess a pKa< pH (**Figure 5B, C and Figure S16 D-F**). In general, the PAs are predicted to transition from ribbons to aggregates (or micelles) with decreasing pH. The pH at which this transition occurs depends on the apparent pK_a of each PA, see inset plots in **Figure 5** and **Figure S16**. Note that the

pK_a of all PAs experience a shift due to the charge regulation effects explained above. The ribbon aggregates of **PA-SO$_3$H** are unfavored for all pH values (**Figure 5B**) because the pKa < pH.[32] This ensures that all sulfonic groups are deprotonated, i.e. $\alpha \sim 1$ for all pH (negative pK_a values will not affect our calculations); ensuring the Coulomb repulsions dominate over the hydrophobic attractive interactions (preventing aggregation).

Structural properties of the twisted ribbons

We have shown that **PA-COOH**, **PA-SO$_3$H**, and **PA-OPO$_3$H$_2$** self-assembled into twisted ribbons at pHs > pKa (**Figure 2**, **PA-CONHCN** also formed twisted ribbons while the other two PAs formed thin ribbons or nanofibers). These structures possess characteristic width (*W*) and twisting pitch (*P*). **Figure 6A** shows the Cryo-TEM of **PA-COOH**. The aggregates formed by these PAs present some polydispersity in both width and period, with values around 10-60 nm and 150-500 nm, respectively. Remarkably, these parameters are not independent from each other. **Figure 6B** shows *P* as a function of *W* for ribbons formed by **PA-COOH**, **PA-SO$_3$H** and **PA-OPO$_3$H$_2$** in PBS buffer (pH = 7.4). *P* and *W* were measured from several cryo-TEM images using the ImageJ software.[43] The plot suggests that there is an approximately linear correlation between *P* and *W*. This correlation has not been reported before for PAs, but it has been previously observed in related self-assembled systems.[44-46]

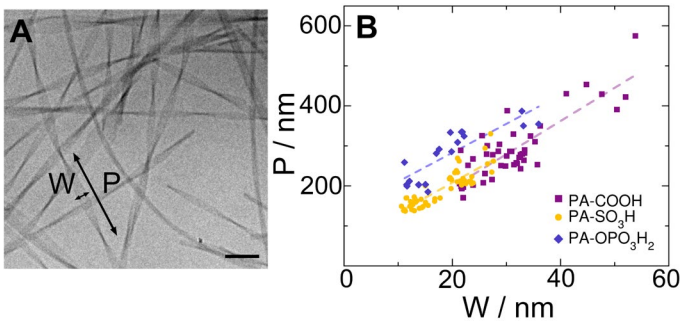


Figure 6. A) Cryo-TEM images of **PA-COOH** in PBS buffer. Double arrows mark the width (W) and pitch (P) of the ribbons (scale bar 100 nm). B) The twisting pitch (P) as a function of the width (W) of twisted ribbons formed by **PA-COOH**, **PA-SO_3H** and **PA-OPO_3H_2** in PBS buffer.

There is reasonable consensus in the literature that the twisting of self-assembled ribbons arises mainly from chiral interactions between the building blocks,[47, 48] with a minor, but not always negligible, contribution of electrostatic interactions.[49-51] The degree of twisting is mainly defined by the competition between a chiral interaction that defines an optimal angle a_0 between two consecutive molecules and an elastic resistance. As a result, an equilibrium angle a^* ($a^* < a_0$) between consecutive molecules arises and propagates in one direction. In PAs, the chiral interactions are presumably peptide-peptide H-bonds influence by the stereochemistry of the side chains, while the elastic resistance is due to the tail-tail hydrophobic attraction that is maximized for the untwisted ribbon. Recently, Zhang *et al.*[44] showed that the positive correlation between the period (P) and width (W) can be understood and quantitatively predicted by a mechanical model that considers such chiral interactions.

Helicoid-shaped ribbons are chiral nanostructures that have either right-handed or left-handed twisting. We used AFM to determine the direction of rotation of the ribbons (**Figures S17 and S18**). The analysis of AFM images supports the hypothesis of the chiral origin of the twisting for two reasons. Firstly, all the ribbons formed by a given PA present the same chirality, which is expected if the twisting arises from the molecular chirality (note we used only *L*-amino acids). Secondly, making isosteric replacements in the PA did not change the macromolecular chirality. This result suggests that the replacements do not significatively affect the packing of consecutive molecules due to peptide-peptide H-bonds. This conclusion is met for the PAs analyzed herein because their acidic groups have similar molecular volumes.

4. Conclusions

We have prepared PAs that contain the same hydrophobic tail and peptide core but possess different anionic groups (carboxylic acid, sulfonic acid, phosphoric acid, methyl sulfonamide, methyl sulfonamide, trifluoromethyl sulfonamide, and cyanamide) to investigate the effect of isosteric replacement (pK_a) on self-assembly. Our data indicates that the self-assembly behavior of PAs is dependent on the pK_a of the ionizable groups. Changes in the solution pH can trigger structural re-arrangements at the supramolecular level. However, if the pK_a value is below the solution's pH, the supramolecular morphology will not be altered. Theoretical studies indicate that this morphological transition is related to changes in the Coulomb repulsions among self-assembled PA nanostructures. The aggregation of those nanostructures occurs when electrostatic repulsions are overcome by hydrophobic attractions. The study on the nanostructure's twisting property indicates that the isosteric replacement does not change the macromolecular chirality. The property of head groups is found to influence the width and twisting of the assembled ribbons, as well as the secondary structure. Moreover, PA nanostructures' thermal stability is related to the morphology of assemblies and physicochemical characters of head groups. This information will be valuable to the development of supramolecular nanostructures with pH-responsive or pH and thermal resistant properties; thus, expanding the potential applications of PA-based nanosystems. Potential future uses of this technology include nanocarriers for oral drug delivery and shape-changing nanostructures to achieve enhanced cell binding, fast clearance, or a burst drug-release. For example, since its shape is unaltered at low pHs (such as the GI environment), **PA-SO_3H**-based nanostructures may be an intriguing option for oral delivery. Meanwhile, the other PAs could change structure in the intestine, pancreas, or duodenum (areas with different pHs) releasing drugs or exposing signaling ligands upon conformational changes.

ASSOCIATED CONTENT

Supporting Information

The SI file contains: the protocol to prepare PA nanostructures; buffer preparation; SAXS model; schematic representation of SAXS; PA chemical structures; Mass spectra; HPLC chromatograms; AFM micrographs for nanostructures; table of measurements of nanoparticles at pH 7.4 by cryo-TEM; table of parameters by SAXS; SAXS patterns at different pHs; nanostructures TEM micrographs at different pHs and salt concentrations; AFM and TEM micrographs with positively charged surface; theoretical studies.

AUTHOR INFORMATION

Corresponding Author

*Martin Conda-Sheridan

E-mail: martin.condasheridan@unmc.edu Tel: +1-402-559-9361.

Present Addresses

[†]Nathalia R Almeida: College of Chemistry, University of Nebraska Omaha, 6001 Dodge Street, Omaha, NE 68182, USA

ORCID

Huihua Xing 0000-0001-7276-6601

Stacey M. Chin 0000-0002-2909-6080

Venkatareddy Udumula 0000-0002-7044-2029

Maddeboina Krishnaiah 0000-0003-2190-4378

Nathalia Rodrigues de Almeida 0000-0002-9552-1233

Cristián Huck-Iriart 0000-0001-5734-2499

Agustín S. Picco 0000-0003-4683-7319

Sieun Ruth Lee 0000-0002-6835-0248

Kelsey A. Jackson 0000-0002-7586-6111

Mario Tagliazucchi 0000-0003-4755-955X

Samuel I. Stupp 0000-0002-5491-7442

Martin Conda-Sheridan 0000-0002-3568-2545

Author Contributions

MC-S conceived the idea and supervised the research. HX performed synthesis (PA-OPO_3H_2), the CD, TEM, AFM experiments, sample preparation and biological assay. SMC and SRL performed and analyzed the cryo-TEM and SAXS. VRU prepared (PA-COOH, PA-SO_3H, and PA-OPO_3H_2), images (TEM and AFM), and CD. MK (PA-$CONHSO_2CH_3$, PA-CONHCN, PA-$CONHSO_2CF_3$, and PA-OPO_3H_2), and KAJ (PA-SO_3H) contributed to synthesis. NRA did synthesis (PA-COOH) and CD. CHI and ASP contributed to the general discussion, suggested experiments, and did (different pH), processed and fitted SAXS patterns. GZ and MT suggested experiments, designed the computational model, analyzed and interpreted the results. SIS contributed to the development of the project and provided access to instrumentation. All authors provided critical comments and helped with manuscript writing.

Funding Sources

Acknowledgment is made to the donors of the American Chemical Society Petroleum Research Fund for support of this research (MC-S, Grant # 57434-DN17) and the National Science Foundation (CAREER, Award # 1941731). This project was also funded by the U.S. Department of Energy, Office of Science, Basic Energy Sciences (Award # DE-SC0000989).

Notes

The authors declare that there are no conflicts of interest.

ACKNOWLEDGMENT

Special thanks to Dr. Liam C. Palmer's for his assistance reading the manuscript and for intellectual input. The X-ray scattering and cryogenic TEM are supported by the Center for Bio-Inspired Energy Science, an Energy Frontier Research Center funded by the U.S. Department of Energy, Office of Science, Basic Energy Sciences under Award # DE-SC0000989. The authors are thankful to the Brazilian Synchrotron Light Laboratory (LNLS-CNPEM) for granting access to SAXS-1 Beamline (proposal SAXS-1 20190212) and the DuPont-Northwestern-Dow Collaborative Access Team (DND- CAT) located at Sector 5 of the Advanced Photon Source (APS). This research used resources of the Advanced Photon Source; a U.S. Department of Energy (DOE) Office of Science User Facility operated for the DOE Office of Science by Argonne National Laboratory under Contract No. DE-AC02-06CH11357. The authors thank Dr. Gaelle Spagnol for technical support. The authors thank the Electron Microscopy Core Facility (EMCF) and Nanoimaging Core Facility at UNMC for experimental assistance. A.S.P, C.H.I and M.T. are CONICET fellows. C.H.I acknowledges funding from ANPCyT (PICT 2017 3150). M.T. acknowledges funding from ANPCyT (PICT 2016 0154) and a CONICET-NIH International Cooperation Grant.

ABBREVIATIONS

PA, peptide amphiphiles; SPPS, solid-phase peptide synthesis; SAXS, small angle X-ray scattering; CD, circular dichroism; TEM, transition electron microscopy; AFM, atomic force microscopy; HPLC, high performance liquid chromatography; MALDI, Matrix Assisted Laser Desorption/Ionization.

Uncategorized References

1. Stephanopoulos, N.; Ortony, J. H.; Stupp, S. I., Self-Assembly for the Synthesis of Functional Biomaterials. *Acta Mater.* **2013,** *61* (3), 912-930.
2. Aida, T.; Meijer, E. W.; Stupp, S. I., Functional Supramolecular Polymers. *Science* **2012,** *335* (6070), 813-7.
3. Whitesides, G. M.; Boncheva, M., Beyond molecules: self-assembly of mesoscopic and macroscopic components. *Proc. Natl. Acad. Sci. U. S. A.* **2002,** *99* (8), 4769-74.
4. Webber, M. J.; Tongers, J.; Renault, M. A.; Roncalli, J. G.; Losordo, D. W.; Stupp, S. I., Development of bioactive peptide amphiphiles for therapeutic cell delivery. *Acta. Biomater.* **2010,** *6* (1), 3-11.
5. Soukasene, S.; Toft, D. J.; Moyer, T. J.; Lu, H.; Lee, H. K.; Standley, S. M.; Cryns, V. L.; Stupp, S. I., Antitumor activity of peptide amphiphile nanofiber-encapsulated camptothecin. *ACS Nano* **2011,** *5* (11), 9113-21.
6. Matson, J. B.; Stupp, S. I., Drug Release from Hydrazone-Containing Peptide Amphiphiles. *Chem. Commun.* **2011,** *47* (28), 7962-4.
7. Rajangam, K.; Behanna, H. A.; Hui, M. J.; Han, X.; Hulvat, J. F.; Lomasney, J. W.; Stupp, S. I., Heparin binding nanostructures to promote growth of blood vessels. *Nano Lett.* **2006,** *6* (9), 2086-90.
8. Shah, R. N.; Shah, N. A.; Del Rosario Lim, M. M.; Hsieh, C.; Nuber, G.; Stupp, S. I., Supramolecular design of self-assembling nanofibers for cartilage regeneration. *Proc. Natl. Acad. Sci. U. S. A.* **2010,** *107* (8), 3293-8.
9. Mata, A.; Geng, Y.; Henrikson, K. J.; Aparicio, C.; Stock, S. R.; Satcher, R. L.; Stupp, S. I., Bone Regeneration Mediated by Biomimetic Mineralization of a Nanofiber Matrix. *Biomaterials* **2010,** *31* (23), 6004-12.
10. Standley, S. M.; Toft, D. J.; Cheng, H.; Soukasene, S.; Chen, J.; Raja, S. M.; Band, V.; Band, H.; Cryns, V. L.; Stupp, S. I., Induction of cancer cell death by self-assembling nanostructures incorporating a cytotoxic peptide. *Cancer Res.* **2010,** *70* (8), 3020-6.
11. Toft, D. J.; Moyer, T. J.; Standley, S. M.; Ruff, Y.; Ugolkov, A.; Stupp, S. I.; Cryns, V. L., Coassembled cytotoxic and pegylated peptide amphiphiles form filamentous nanostructures with potent antitumor activity in models of breast cancer. *ACS Nano* **2012,** *6* (9), 7956-65.
12. Rodrigues de Almeida, N.; Han, Y.; Perez, J.; Kirkpatrick, S.; Wang, Y.; Sheridan, M. C., Design, Synthesis, and Nanostructure-Dependent Antibacterial Activity of Cationic Peptide Amphiphiles. *ACS Appl. Mater. Inter.* **2018,** *11*, 2790.
13. Hartgerink, J. D.; Beniash, E.; Stupp, S. I., Self-assembly and mineralization of peptide-amphiphile nanofibers. *Science* **2001,** *294* (5547), 1684-8.
14. Dehsorkhi, A.; Castelletto, V.; Hamley, I. W., Self-assembling amphiphilic peptides. *J. Pept. Sci.* **2014,** *20* (7), 453-67.
15. Lowik, D. W.; van Hest, J. C., Peptide Based Amphiphiles. *Chem. Soc. Rev.* **2004,** *33* (4), 234-45.
16. Tantakitti, F.; Boekhoven, J.; Wang, X.; Kazantsev, R. V.; Yu, T.; Li, J.; Zhuang, E.; Zandi, R.; Ortony, J. H.; Newcomb, C. J.; Palmer, L. C.; Shekhawat, G. S.; de la Cruz, M. O.; Schatz, G. C.; Stupp, S. I., Energy landscapes and functions of supramolecular systems. *Nat. Mater.* **2016,** *15* (4), 469-76.
17. Moyer, T. J.; Finbloom, J. A.; Chen, F.; Toft, D. J.; Cryns, V. L.; Stupp, S. I., pH and amphiphilic structure direct supramolecular behavior in biofunctional assemblies. *J. Am. Chem. Soc.* **2014,** *136* (42), 14746-52.

18. Korevaar, P. A.; Newcomb, C. J.; Meijer, E. W.; Stupp, S. I., Pathway Selection in Peptide Amphiphile Assembly. *J. Am. Chem. Soc.* **2014,** *136* (24), 8540-3.
19. Ghosh, A.; Buettner, C. J.; Manos, A. A.; Wallace, A. J.; Tweedle, M. F.; Goldberger, J. E., Probing Peptide Amphiphile Self-Assembly in Blood Serum. *Biomacromolecules* **2014,** *15* (12), 4488-4494.
20. Buettner, C. J.; Wallace, A. J.; Ok, S.; Manos, A. A.; Nicholl, M. J.; Ghosh, A.; Tweedle, M. F.; Goldberger, J. E., Balancing the Intermolecular Forces in Peptide Amphiphiles for Controlling Self-Assembly Transitions. *Org. Biomol. Chem.* **2017,** *15* (24), 5220-5226.
21. Ozkan, A. D.; Tekinay, A. B.; Guler, M. O.; Tekin, E. D., Effects of temperature, pH and counterions on the stability of peptide amphiphile nanofiber structures. *RSC Adv.* **2016,** *6* (106), 104201-104214.
22. Toksoz, S.; Mammadov, R.; Tekinay, A. B.; Guler, M. O., Electrostatic effects on nanofiber formation of self-assembling peptide amphiphiles. *J .Colloid. Interface. Sci.* **2011,** *356* (1), 131-7.
23. Cote, Y.; Fu, I. W.; Dobson, E. T.; Goldberger, J. E.; Nguyen, H. D.; Shen, J. K., Mechanism of the pH-Controlled Self-Assembly of Nanofibers from Peptide Amphiphiles. *J. Phys. Chem. C* **2014,** *118* (29), 16272-16278.
24. Zaldivar, G.; Vemulapalli, S.; Udumula, V.; Conda-Sheridan, M.; Tagliazucchi, M., Self-Assembled Nanostructures of Peptide Amphiphiles: Charge Regulation by Size Regulation. *J. Phys. Chem. C* **2019,** *123* (28), 17606-17615.
25. Lin, B. F.; Marullo, R. S.; Robb, M. J.; Krogstad, D. V.; Antoni, P.; Hawker, C. J.; Campos, L. M.; Tirrell, M. V., De Novo Design of Bioactive Protein-Resembling Nanospheres via Dendrimer-Templated Peptide Amphiphile Assembly. *Nano Lett.* **2011,** *11* (9), 3946-3950.
26. Andrievskii, R., Review Stability of Nanostructured Materials. *J. Mater. Sci.* **2003,** *38*, 1367-1375.
27. Chen, C. H.; Palmer, L. C.; Stupp, S. I., Self-Repair of Structure and Bioactivity in a Supramolecular Nanostructure. *Nano Lett.* **2018,** *18* (11), 6832-6841.
28. Lassalas, P.; Gay, B.; Lasfargeas, C.; James, M. J.; Tran, V.; Vijayendran, K. G.; Brunden, K. R.; Kozlowski, M. C.; Thomas, C. J.; Smith, A. B.; Huryn, D. M.; Ballatore, C., Structure Property Relationships of Carboxylic Acid Isosteres. *J. Med. Chem.* **2016,** *59* (7), 3183-3203.
29. Garvey, D. S.; Wasicak, J. T.; Elliott, R. L.; Lebold, S.; Hettinger, A.-M.; Carrera, G. M.; Lin, N.-H.; He, Y.; Holladay, M. W., Ligands for Brain Cholinergic Channel Receptors: Synthesis and in Vitro Characterization of Novel Isoxazoles and Isothiazoles as Bioisosteric Replacements for the Pyridine Ring in Nicotine. *J. Med. Chem.* **1994,** *37* (26), 4455-4463.
30. Samad, M. B.; Chhonker, Y. S.; Contreras, J. I.; McCarthy, A.; McClanahan, M. M.; Murry, D. J.; Conda-Sheridan, M., Developing Polyamine-Based Peptide Amphiphiles with Tunable Morphology and Physicochemical Properties. *Macromol. biosci.* **2017,** *17* (8), 10.1002/mabi.201700096.
31. Maldonado, L.; Debais, G.; Davia, F.; Méndez De Leo, L. P.; Tagliazucchi, M., Interpolymer Complexes of Poly(sulfonic acid)s and Poly(ethylene oxide): an Unexpected Association. *Soft Matter* **2019,** *15* (45), 9318-9324.
32. Guthrie, J. P., Hydrolysis of esters of oxy acids: pKa values for strong acids; Brønsted relationship for attack of water at methyl; free energies of hydrolysis of esters of oxy acids; and a linear relationship between free energy of hydrolysis and pKa holding over a range of 20 pK units. *Can. J. Chem.* **1978,** *56* (17), 2342-2354.

33. Dong, H.; Du, H.; Wickramasinghe, S. R.; Qian, X., The Effects of Chemical Substitution and Polymerization on the pKa Values of Sulfonic Acids. *J. Phys. Chem. B* **2009,** *113* (43), 14094-14101.
34. Rayne, S.; Forest, K., Estimated pKa values for the environmentally relevant C1 through C8 perfluorinated sulfonic acid isomers. *J. Environ. Sci. Health A Tox. Hazard Subst. Environ. Eng.* **2016,** *51* (12), 1018-23.
35. Powell, K. J.; Brown, P. L.; Byrne, R.; Gajda, T.; Hefter, G.; Sjöberg, S.; Wanner, H., Chemical speciation of environmentally significant heavy metals with inorganic ligands part 1: The Hg2+- Cl-, OH-, CO32-, so42-, and PO 43- aqueous systems. *Pure Appl. Chem.* **2005,** *77*, 739-800.
36. Mock, W. L.; Xu, X. D., Catalytic Hydrolysis of Acylcyanamide Substrates by Carboxypeptidase A Defines the Stereochemistry of Carbonyl Hydration at the Enzyme Active Site. *Bioorg. Chem.* **1994,** *22* (4), 373-386.
37. Gabor, K. A.; Stevens, C. R.; Pietraszewski, M. J.; Gould, T. J.; Shim, J.; Yoder, J. A.; Lam, S. H.; Gong, Z.; Hess, S. T.; Kim, C. H., Super resolution microscopy reveals that caveolin-1 is required for spatial organization of CRFB1 and subsequent antiviral signaling in zebrafish. *PLoS One* **2013,** *8* (7), e68759.
38. Feigin, L. A.; Svergun, D. I.; Taylor, G. W., Determination of the Integral Parameters of Particles. In *Structure Analysis by Small-Angle X-Ray and Neutron Scattering*, Feigin, L. A.; Svergun, D. I.; Taylor, G. W., Eds. Springer US: Boston, MA, 1987; pp 59-105.
39. Hammouda, B., A new Guinier–Porod model. *J. Appl. Cryst.* **2010,** *43* (4), 716-719.
40. Cui, H.; Muraoka, T.; Cheetham, A. G.; Stupp, S. I., Self-Assembly of Giant Peptide Nanobelts. *Nano Letters* **2009,** *9* (3), 945-951.
41. Pashuck, E. T.; Cui, H.; Stupp, S. I., Tuning Supramolecular Rigidity of Peptide Fibers through Molecular Structure. *J. Am. Chem. Soc.* **2010,** *132* (17), 6041-6046.
42. Gao, C.; Li, H.; Li, Y.; Kewalramani, S.; Palmer, L. C.; Dravid, V. P.; Stupp, S. I.; Olvera de la Cruz, M.; Bedzyk, M. J., Electrostatic Control of Polymorphism in Charged Amphiphile Assemblies. *J. Phys. Chem. B* **2017,** *121* (7), 1623-1628.
43. Schneider, C. A.; Rasband, W. S.; Eliceiri, K. W., NIH Image to ImageJ: 25 years of image analysis. *Nat. Methods* **2012,** *9* (7), 671-675.
44. Zhang, M.; Grossman, D.; Danino, D.; Sharon, E., Shape and fluctuations of frustrated self-assembled nano ribbons. *Nat. Commun.* **2019,** *10* (1), 3565.
45. Ziserman, L.; Mor, A.; Harries, D.; Danino, D., Curvature Instability in a Chiral Amphiphile Self-Assembly. *Phys. Rev. Lett.* **2011,** *106* (23), 238105.
46. Nakai, T.; Sugano, Y.; Shoda, M.; Sakakibara, H.; Oiwa, K.; Tuzi, S.; Imai, T.; Sugiyama, J.; Takeuchi, M.; Yamauchi, D.; Mineyuki, Y., Formation of Highly Twisted Ribbons in a Carboxymethylcellulase Gene-Disrupted Strain of a Cellulose-Producing Bacterium. *J. Bacteriol.* **2013,** *195* (5), 958.
47. Zhang, L.; Wang, T.; Shen, Z.; Liu, M., Chiral Nanoarchitectonics: Towards the Design, Self-Assembly, and Function of Nanoscale Chiral Twists and Helices. *Adv. Mater.* **2016,** *28* (6), 1044-1059.
48. Shimizu, T.; Masuda, M.; Minamikawa, H., Supramolecular nanotube architectures based on amphiphilic molecules. *Chem. Rev.* **2005,** *105* (4), 1401-43.
49. Assenza, S.; Adamcik, J.; Mezzenga, R.; De Los Rios, P., Universal Behavior in the Mesoscale Properties of Amyloid Fibrils. *Phys. Rev. Lett.* **2014,** *113* (26), 268103.

50. Zaldivar, G.; Conda-Sheridan, M.; Tagliazucchi, M., Twisting of Charged Nanoribbons to Helicoids Driven by Electrostatics. *J. Phys. Chem. B* **2020,** *124* (15), 3221-3227.
51. Uesaka, A.; Ueda, M.; Makino, A.; Imai, T.; Sugiyama, J.; Kimura, S., Morphology Control between Twisted Ribbon, Helical Ribbon, and Nanotube Self-Assemblies with His-Containing Helical Peptides in Response to pH Change. *Langmuir* **2014,** *30* (4), 1022-1028.

TOC Graphic

